Positron implantation-profile effects in solids*

Werner Brandt† and Robert Paulin
Institut National des Sciences et Techniques Nucléaires, Saclay, France
(Received 10 June 1976)

A method is developed to measure positron implantation profiles in solids and the changes induced by anisotropies or externally applied electric fields through the dependence on depth, x, of positron-electron annihilations. The implantation profiles, $P_+(x)$, of positrons from ^{64}Cu sources, with maximum kinetic energy 0.65 MeV, in 14 different solids, ranging in density d (g/cm^3) from 0.9 to 9, can be described by $P_+(x) = \exp(-x/R_+)$, with a mean implantation range R_+ (0.65 MeV) = $(345 \pm 25) d^{-1}$ (μm). Compared to polycrystalline samples, R_+ increases by 10% in Cu single crystals under channeling conditions along the ⟨110⟩ direction. The measured displacements of $P_+(x)$ in C (diamond) and Si crystals induced by electric fields up to 5 kV/cm give positron mobilities 200 to 400 cm^2/Vsec, which are 5 to 10 times smaller than the corresponding electron mobilities. Profiles of lattice defects induced in NaCl crystals by x rays of various energies are measured through positron trapping, as signified by x-dependent changes of the angular correlation between the annihilation γ rays.

I. INTRODUCTION

This paper reports measurements of positron transport coefficients and annihilation properties in surface domains of solids. They are based on the fact that positrons, when injected into a solid or liquid, reach thermal energies in times short compared to their lifetimes, and diffuse over distances very small compared to their mean ranges before they annihilate with an electron into γ quanta.[1] In this sense, the site of annihilation coincides with the site of positron implantation.

Almost all positrons implanted in condensed matter annihilate with an electron into two γ quanta each of energy $m_0c^2 = 0.511$ MeV, m_0 being the electron rest mass and c the velocity of light. The γ rays emerge from the annihilation site in nearly opposite directions to conserve momentum. Deviations from π radian of the two-γ angular correlations of the order of $v_0/c = 1/137 = 7$ mrad, v_0 being the Bohr velocity, are a measure of the momentum distribution of the electrons sampled by the positron wave function in the material. The equivalent electron energy distribution is measured through the Doppler shifts of the 0.511-MeV annihilation γ rays.

The number of β particles from radioactive sources emerging from foils of thickness x decreases very nearly exponentially with x. We assume that the positron implantation profile, $P_+(x)$, inside a sample can be described to leading terms by

$$P_+(x) = e^{-\alpha_+ x}, \tag{1}$$

where the absorption coefficient

$$\alpha_+ = \lim_{x\to 0}\left(\frac{-d \ln P_+(x)}{dx}\right) \tag{2}$$

defines a practical mean positron implantation range $R_+ \equiv \alpha_+^{-1}$, which depends on the sample-mass density d(g/cm^3) and the maximum energy E_{+M} (MeV) of the positron spectrum as

$$\alpha_+ \equiv R_+^{-1} = C_+ d/E_{+M}^{\beta_+} \text{ cm}^{-1}, \tag{3}$$

with empirical parameters C_+ and β_+. Transmission experiments with radioactive electron sources yield the values $C_- = 17.0$ cm^2/g and $\beta_- = 1.43$ independent of the atomic number Z of the medium.[2]

Given the implantation profile in a material, one may impose experimental conditions which cause positron implantation-profile effects (PIPE) that change either the profile, or the annihilation conditions over distances comparable to R_+, or both. Positron implantation-profile measurements were first performed by Page and Heinberg.[3] Orth[4] observed a shift in the implantation profile in glass under the influence of an electric field. We report positron implantation profiles and measure profile effects as a function of sample structure in Cu, applied electric fields in Si and C (diamond), and radiation-produced defect formation in NaCl. The following Sec. II describes the apparatus, data analysis, and material properties. Section III presents the measured positron implantation profiles in 14 materials. Section IV reports and discusses the data on implantation-profile effects. The results are summarized in Sec. V.

II. EXPERIMENTAL

Figure 1 shows our instrument which is a modified two-γ angular-correlation spectrometer described elsewhere.[5] A 1-Ci ^{64}Cu ($E_{+M} = 0.65$ MeV; half-life 12.9 h) positron source and a sample on a platform can be advanced with a micrometer screw relative to the plane defined by the stationary lead slits. The source is separated from the sample by a spacer with an inner diameter so

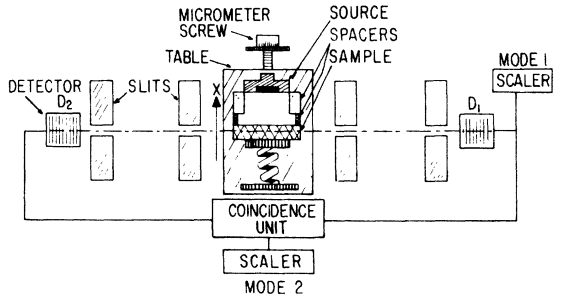

FIG. 1. Apparatus for positron implantation effect (PIPE) measurements in Mode 1 and Mode 2, as described in the text (schematic and not to scale).

wide (1 cm) that only a small fraction of annihilations occurs in the spacer. A second 1-mm-long wider spacer is blocked from the positron source by the first spacer, and reduces counts from backscattered positrons.[6] The count rate when the slit plane intersects this second spacer establishes the reference noise level. The temperature of the assembly was kept constant to $<1\,^{\circ}C$, to suppress changes in the position of the positron entrance surface of the sample relative to the slit system.

A. Mode 1

An NaI(Tl) scintillation counter mounted on a 53 AVP photomultiplier, D_1, registers the 0.511-MeV γ rays which pass through two aligned long slits from a sample layer of mean thickness Δ at a given position x of the source-sample assembly. The first slit, a collimator, is placed 25 cm and the second 200 cm from the sample. The slit widths are typically 0.1 mm. The slit plane is oriented parallel to the positron entrance surface and intercepts, at x, the sample fixed to a movable table. The counting of annihilation γ quanta as a function of x in this manner is referred to as experimental Mode 1 (M1). The detector count rate, $N_1(x)$, in M1 is a direct measure of $P_+(x)$ and yields α_+. In our experiments with relatively short-lived (12.9-h) ^{64}Cu sources, a second detector monitored the source and stopped the run after a preset number of counts, at which time the number of counts $N_1(x)$ registered by D_1 is stored. The sample-source platform is advanced, and a new run started.

Figure 2 shows an M1 sweep of a source quartz-sample assembly by increments of 0.1 mm, starting from a position outside the source. After passing the source, the count rate drops sharply over a displacement comparable to the geometrical width Δ of the layer seen by D_1 ($\sim$0.13 mm in Fig. 2), and remains constant over the extension of the first spacer. At the second spacer, made here of Al ($Z=13$), the count rate drops further to a value B which is taken to be the noise level for all data. As the slit plane passes the surface of the quartz sample located at $x=x_S$, N_1 rises over a distance $\sim\Delta$ to a maximum and decreases exponentially until it levels off toward the noise plateau. Unfolding of such data with the resolution function of the detector system yields the positron implantation profile in the sample.

B. Mode 2

Two identical scintillation photomultiplier detectors and slit systems D_1 and D_2 in coincidence view a sample layer of width Δ. In Mode 2 (M2) therefore, they are in effect a position-sensitive π-radian coincidence apparatus (PICA) which measures the angular correlation between the two 0.511-MeV γ rays that emerge from the annihilation of positrons with electrons, with an acceptance angle limited to values close to π rad. An increase in the PICA count rate $N_P(x)$ can determine the fraction of positrons that annihilate in crystal defects created by some treatment such as irradiation or heat, where they encounter electrons of lower momenta than in the bulk of the material.[1] The coincidence rate $N_P(x)$, in M2 is a measure of the annihilation conditions throughout the surface domain probed by the positrons with probability $P_+(x)$. An equivalent M2 experiment would be the measurement of the x dependence of the Doppler shifts and count rates of 0.511-MeV γ rays emanating from a layer at x. The fraction of annihilations from the positrons deposited at x into the PICA mode is given by $N_2(x)$ defined as

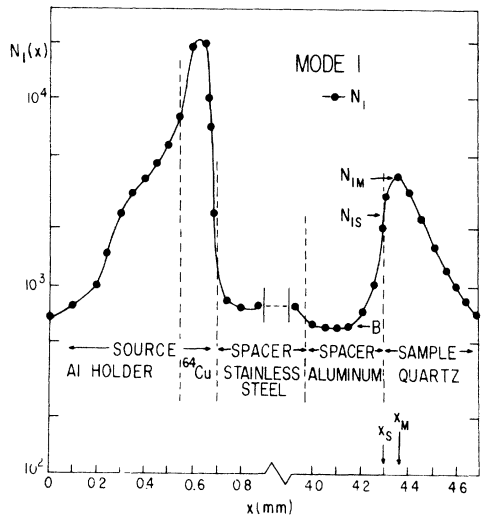

FIG. 2. Illustrative mode-1 sweep of an assembly with a ^{64}Cu source and a quartz sample.

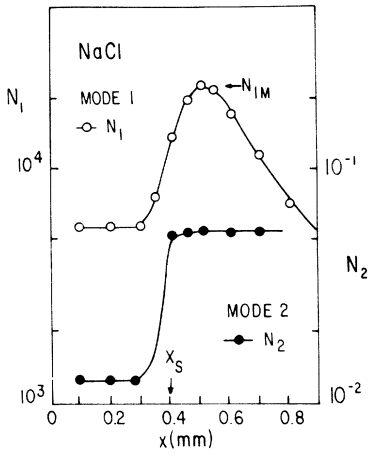

FIG. 3. Mode-1 and mode-2 sweeps of a NaCl crystal.

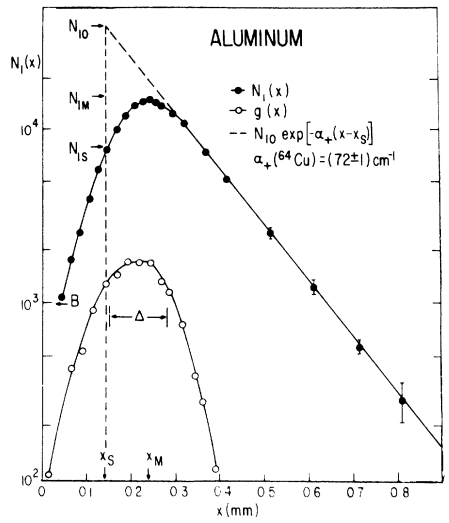

FIG. 4. Mode-1 sweep of a polycrystalline Al sample. The $N_1(x)$ data are decomposed into the instrument resolution function, $g(x)$ of width Δ, and the implantation profile $N_{10}e^{-\alpha_+(x-x_S)}$ for ^{64}Cu positrons.

$N_2(x) \equiv N_P(x)/N_1(x)$, which is recorded directly.

The M1 and M2 curves for a NaCl crystal are displayed in Fig. 3. The ratio of the N_2 levels is equal to the inverse ratio of the widths of the angular correlation curves of the spacer material[7] Fe and of the NaCl sample. In homogeneous isotropic samples, N_2 does not change with x when $x > x_S$, though the statistical uncertainty rises as the number of implanted positrons decreases exponentially with x.

C. Analysis

One can extract the resolution function $g(x, \Delta)$ of the detector system of slit width Δ from N_1 data, with Eq. (1) as the trial function for $P_+(x)$,

$$N_1(x) = B\int_{-\infty}^{x_S} g(x'-x)\,dx' + M\int_{x_S}^{\infty} g(x'-x)e^{-\alpha_+ x'}\,dx', \tag{4}$$

where B is the noise level in the spacer, x_S is the as yet unknown position of the sample surface, and M is a constant. With $N_1'(x) \equiv dN_1(x)/dx$, inversion of Eq. (4) in the limit of high signal-to-noise ratios, $M/B \gg 1$, yields

$$g(x) = M^{-1}[N_1'(x) + \alpha_+ N_1(x)], \tag{5}$$

where M normalizes $\int_{-\infty}^{+\infty} g(x)dx = 1$, and α_+ is the slope of the data $[N_1(x) - B]$ for x large compared to x_M, the position of the maximum $N_1(x_M) \equiv N_{1M}$.

The position of the sample surface x_S appears as a fit parameter in Eq. (4). It can be located relative to x_M by determining N_{1S},

$$N_{1S} \equiv N_1(x = x_S) \simeq \tfrac{1}{2}B + (M/\alpha_+\Delta)(1 - e^{-\alpha_+\Delta/2}), \tag{6}$$

relative to the observed

$$N_{1M} \equiv N_1(x = x_M) \simeq (M/\alpha_+\Delta)(1 - e^{-\alpha_+\Delta}), \tag{7}$$

so that

$$N_{1S} \simeq \frac{1}{2}\left(B + 2\,\frac{1 - e^{-\alpha_+\Delta/2}}{1 - e^{-\alpha_+\Delta}}\,N_{1M}\right), \tag{8}$$

from which the position of the surface can be ascertained. In the Al experiments shown in Fig. 4, the conditions were such that $\alpha_+\Delta \sim 1$, and therefore $N_{1S} \simeq \frac{1}{2}(B + 1.25N_{1M})$, as confirmed by a detailed computer analysis of the data. In the limits $M/B \gg 1$ and $\alpha_+\Delta \ll 1$, Eq. (8) simplifies to $N_{1S} = \frac{1}{2}N_{1M}$.

When electric fields are applied along the implantation direction in materials with negligible internal polarization, all positrons experience the same electric field $\mathcal{E}$, and move with drift velocity $v_d(\mathcal{E})$ over the same mean distance $v_d\tau_c$ before annihilation with lifetime τ_c. The drift velocity is related to the field strength as $v_d = -\mu_+\mathcal{E}$, where μ_+ is the positron mobility. The relative change $\Delta N_1/N_1$ of the count rates with field on and field off at positions $x > x_S + (\frac{1}{2}\Delta)$ is given by

$$\frac{\Delta N_1(\mathcal{E})}{N_1(0)} \equiv \frac{N_1^{on}}{N_1^{off}} - 1 = \int_{x_S}^{+\infty} dx' \int_0^{\infty} dt\, g(x'-x,\Delta)\, e^{-\alpha_+(x'+v_d t)} e^{-t/\tau_c} \left(\int_{x_S}^{+\infty} dx' \int_0^{\infty} dt\, g(x'-x,\Delta)\, e^{-\alpha_+ x'} e^{-t/\tau_c}\right)^{-1} - 1$$

$$\simeq -\frac{\alpha_+\tau_c v_d}{1 + \alpha_+\tau_c v_d} \simeq \alpha_+\tau_c\mu_+\mathcal{E}, \tag{9}$$

TABLE I. Single crystals used in PIPE measurements.

Crystal	Implantation direction	Origin
NaCl	unknown	Quartz et Silice, France
Si [a]	⟨110⟩	Hoboken, Belgium
quartz	z axis	Lammon, France
Zr	unknown	I.N.S.T.N., France [b]
Cu	⟨110⟩	Cristal Tec, France

[a] p-type, internal resistance 3 kΩ cm.
[b] Courtesy J. C. Couterne. Confer G. Coussot, Phys. Rev. B 3, 1048 (1971).

from which μ_+ can be determined. Since Eq. (9) is independent of x and Δ, one can measure μ_+ with wide slits or merely a jaw placed to block the detector from the γ rays emanating in the positron-entrance layer of thickness $\gg v_d\tau_c$. This optimizes the statistical accuracy of the relative differences between N_1^{on} and N_1^{off}.

D. Materials

Polycrystalline samples were prepared as disks, ~1-cm diameter and 0.5 cm thick, of commercial high-purity grade materials. The single crystals used in implantation profile measurements are listed in Table I.

Positron mobilities were measured in a 1.3 carat monocrystal of type-IIa diamond of dimensions 9.5 × 4 × 2 mm, with the ⟨111⟩ axis along the implantation direction.[8] Gold electrodes approximately 100 Å thick were evaporated onto the two 9.5 × 4 mm surfaces. The positron entrance surface was in contact with one electrode of a variable stabilized power supply, and the back surface through a micro-ampere meter with the other electrode. After each measurement at a position x, the polarity of the voltage was reversed and a second measurement performed to give $2\Delta N_1(x)/N_1(x)$.

Positron mobility measurements in Si were performed on Li-drifted Si detectors of identical structure: diameter 20 mm, thickness of compensated layer 3.8 mm, of n layer 200 μm, of p layer 1 μm, and covered with a 100-Å Au electrode.[9] For PIPE measurements a Si crystal was mounted in the sample holder with reverse polarity. The polarity could not be interchanged here, and the low internal resistance limited the voltage that could be applied without undue heating of the Si samples. Without the positron source, the current was 10 μA at 2000 V and 30 μA at 3000 V; with the positron source, it was typically 50 μA at 2000 V and 80 μA at 3000 V. The electric field in the implantation layer was taken to be equal to the applied voltage divided by the thickness 3.8 mm of the compensated layer.

III. IMPLANTATION PROFILES

Mode 1 measurements were performed two or three times each on samples of 13 different materials. The deconvoluted average data are shown in Fig. 5 in a semilogarithmic plot of $P_+(x)$ vs xd. A fit to all data yields the mean value $\alpha_+/d = 29 \pm 1$ cm²/g. With $E_{+M}(^{64}\mathrm{Cu}) = 0.65$ MeV and by setting $\beta_+ = \beta_- = 1.43$, we calculate the constant $C_+ = 16 \pm 1$ cm²/g as compared to $C_- = 17.0 \pm 0.3$ cm²/g deduced from electron-transmission measurements.[2] That is, at $E_M = 0.65$ MeV, the implantation ranges of positrons and electrons from radioactive sources are essentially equal. The total ranges of monoenergetic positrons and electrons calculated in the continuous slowing-down approximation[10,11]

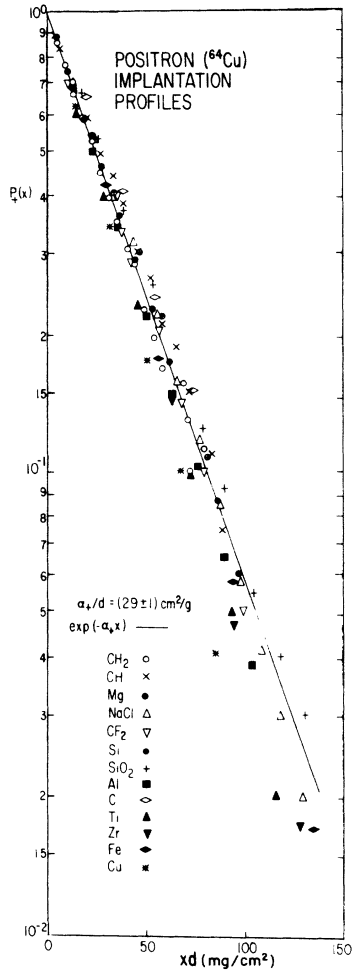

FIG. 5. Normalized implantation profiles of positrons from ^{64}Cu ($E_{+M} = 0.65$ MeV), measured in mode 1 for 13 materials, as a function of the implantation surface density xd (in mg/cm²). The solid line represents Eq. (1) with $\alpha_+(^{64}\mathrm{Cu})/d = 29$ cm²/g. Best α_+ values of the different materials are listed in Table II.

TABLE II. Positron mass absorption coefficients measured with positrons from ^{64}Cu sources, with maximum positron energy 0.65 MeV, in various materials. Samples marked with an asterisk (*) were single crystals, the other polycrystalline. The mean value for all samples, $\alpha_+/d = 29 \pm 1$ cm^2/g, corresponds to a mean positron implantation range $R_+(0.65\ \text{MeV}) \equiv \alpha_+^{-1} = [(345 \pm 12) d^{-1}$ (g/cm^3)] μm.

Material	d (g/cm^3)	α_+ (cm^{-1})	α_+/d (cm^2/g)
polyethylene (CH_2)	0.9	27 ± 1.5	30 ± 2
anthracene (CH)	1.25	33 ± 2.0	26 ± 2
Mg ($Z=12$)	1.74	48 ± 1.2	28 ± 1
NaCl	2.14	60 ± 2.0	28 ± 1
Teflon (CF_2)	2.22	64 ± 2.5	29 ± 1
Si ($Z=14$)*	2.33	63 ± 2.5	27 ± 1
quartz (SiO_2)*	2.65	71 ± 3.0	27 ± 1
Al ($Z=13$)	2.70	72 ± 2.0	27 ± 1
diamond ($Z=6$)	3.51	95 ± 10	27 ± 3
Ti ($Z=22$)	4.54	150 ± 9.0	33 ± 2
Zr ($Z=40$)*	6.53	210 ± 20	32 ± 3
Fe ($Z=26$)	7.92	250 ± 20	32 ± 3
Cu ($Z=27$)	8.92	303 ± 20	34 ± 2
Cu ($Z=27$)*	8.92	278 ± 20	32 ± 2

happen to be equal at 0.65 MeV. Most ^{61}Cu positrons have lower energies, at which positron ranges are shorter than electron ranges (they are longer at higher energies). On these grounds the ratio R_+/R_- should be less than unity. Apparently multiple scattering compensates for differences in the slowing-down rates. Measurements with various positron sources are necessary to test this observation further.

The data in Fig. 5 do not resolve any significant systematic deviations from Eqs. (1) and (3) in their dependence on xd. Separate fits of Eq. (1) to the data of a given material are collated in Table II. Barely resolved trends appear, viz., α_+/d values grow as the atomic number Z of the samples, perhaps as $Z^{1/3}$, and α_+/d values are smaller in single crystals than in polycrystalline samples. They deserve further study. A detailed comparison of M1 data of a Cu crystal and a polycrystalline sample is given in Sec. IV.

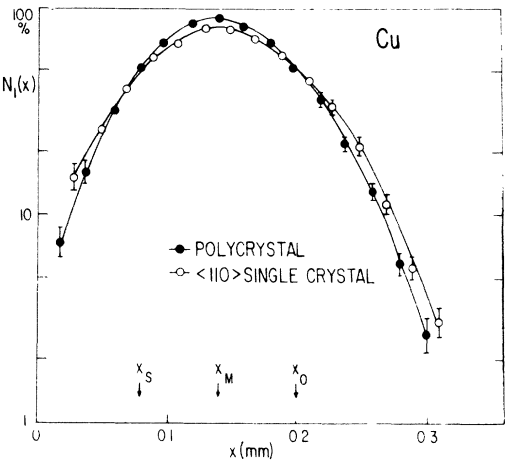

FIG. 6. Mode 1 sweeps through a polycrystalline and a single-crystal Cu sample. The positions of the maxima coincide within < 0.01 mm, and are taken to be equal. The difference curve is shown in Fig. 7.

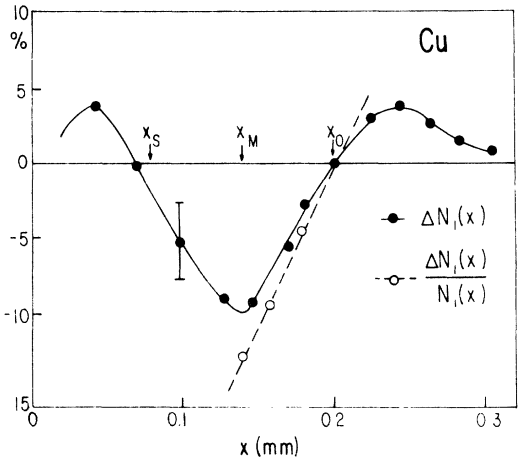

FIG. 7. Difference curve of $N_1(x)$ counts (solid points) in a single crystal (positron entrance direction along ⟨110⟩ crystal direction) and a polycrystalline sample of Cu (cf. Fig. 6). The slope of the dashed line, $\Delta N_1(x)/N_1(x)$ (open circles) that connects between $x = x_M$ and the position $x = x_0$ where $\Delta N_1(x)/N_1(x) = 0$, gives $\delta\alpha_+ = -2.5$ mm^{-1}.

IV. POSITRON IMPLANTATION EFFECTS

A. Positron channeling in Cu

Precision M1 measurements were made on two Cu slabs with polished and etched surfaces. One was a polycrystalline sample, and the other a monocrystal with the ⟨110⟩ direction parallel to the positron entrance direction x. The M1 data as compared in Fig. 6 are normalized to the same number of counts. In terms of the N_{1M} values and the position $x = x_0 > x_M$ where $\Delta N_1(x_0) = 0$, one obtains

$$\delta\alpha_+ = (x_0 - x_M)^{-1}(\Delta N_{1M}/N_{1M}). \quad (10)$$

Figure 7 displays $\Delta N_1(x)$ from which we determine by analysis $\delta\alpha_+ = -25$ cm^{-1}. The mean ^{64}Cu positron implantation range in the ⟨110⟩ direction of a Cu crystal is thus approximately 3 μm longer than $R_+ = 33$ μm in polycrystalline Cu. This implies, e.g., that if the channeling range were $2R_+$, some 10% of all positrons channel in the crystal.

We found no evidence for "supertails" in the

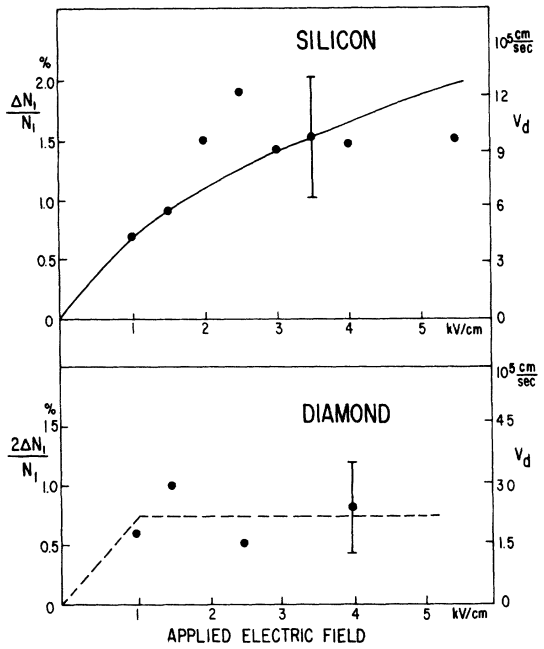

FIG. 8. Relative shifts of positron annihilation profiles $\Delta N_1/N_1$, and positron drift velocities v_d, in electric fields $\mathcal{E}$. The uncertainties are indicated by representative error bars. The solid curve in the upper graph represents Eq. (12) with $\mathcal{E}_c = 2$ kV/cm and $\mu_+ = 430$ cm^2/V sec. The dashed line in the lower graph gives the positron-trapping limited drift velocity for 10-ppm trapping centers in this diamond. The drift velocity rises at lower fields as sketched in the figure with a positron mobility ~200 cm^2/V sec.

implantation profiles due to positrons that, after implantation in a crystal channel, diffuse deep into the crystal beyond the range of channel implantation. In fact, supertails should not appear as a distinct phenomenon even for collimated monoenergetic positron beams. In terms of the positron diffusion constant D_+ and lifetime τ_c, the diffusion length is $\Lambda_+ = (2D_+\tau_c)^{1/2}$. Thermal positrons have a de Broglie wavelength, ~12 Å, large compared to lattice constants, and diffuse over distances, Λ_+, so short that $\alpha_+\Lambda_+ \ll 1$, whether implanted along channels or in random directions. Thus positron diffusion, as a small integral part of the implantation range, remains unaffected by channeling conditions.

B. Positron mobilities

Electric-field M1 experiments were performed on Si and C (diamond monocrystals) as described in Sec. II. The results are shown in Fig. 8 relative to the left ordinate scales, $\Delta N_1/N_1$ for Si in the upper graph, and $2\Delta N_1/N_1$ for diamond in the lower graph. An early measurement of electric-field effects on the angular correlation[12,13] of diamond gave the mobility $\mu_+ = 120 \pm 160$ cm^2/V sec, and so indicated essentially zero mobility of positrons if compared with $\mu_-(C) \sim 1500$–2000 cm^2/V sec for electrons in diamond.[14] The 300 °K electron mobility in Si crystals is $\mu_-(\mathrm{Si}) \sim 1400$ cm^2/V sec.[15]

The right ordinates in Fig. 8 give the scale of the corresponding positron drift velocities v_d, calculated by Eq. (9),

$$v_d(\mathcal{E}) = (\alpha_+\tau_c)^{-1}[\Delta N_1(\mathcal{E})/N_1], \tag{11}$$

with the α_+ values given in Table II and $\tau_c(\mathrm{Si}) = 230$ psec,[16] $\tau_c(\mathrm{diamond}) = 184$ psec.[17] The drift velocities are comparable to the sound velocities, u [$u(\mathrm{Si}) = 7 \times 10^5$ cm/sec; $u(\mathrm{diamond}) = 8 \times 10^5$ cm/sec]. We write Shockley's theory[18] of the drift velocity of nondegenerate charge carriers in semiconductors for positrons in the form

$$v_d(\mathcal{E}) = \frac{\sqrt{2}\,\mu_+\mathcal{E}}{\{1+[1+(2\mathcal{E}/\mathcal{E}_c)^2]^{1/2}\}^{1/2}} = \begin{cases} \mu_+\mathcal{E} & \text{when } \mathcal{E} \ll \mathcal{E}_c, \\ \mu_+\mathcal{E}_c^{1/2}\,\mathcal{E}^{1/2} & \text{when } \mathcal{E} \gg \mathcal{E}_c, \end{cases} \tag{12}$$

where μ_+ is the low-field $\mathcal{E}$-independent mobility. The critical field strength $\mathcal{E}_c \equiv (32/3\pi)^{1/2}(u/\mu_+)$ is a material constant. In the phonon-limited regime, $\mathcal{E} \ll \mathcal{E}_c$, μ_+ has the form $\mu_+ = \mu_{0+}(T_0/T)^{3/2}$ in a crystal lattice of temperature T, where μ_{0+}, T_0 are constants.[19] We estimate that Joule heating raised the internal Si temperature from ~310 °K at 2 kV/cm to ~360 °K at 4 kV/cm, which lowered the positron drift velocity throught positron-phonon scattering by a factor approximately $(310/360)^{3/2} = 0.8$ at the high fields relative to that expected in a sample of constant temperature. With this correction, the Si points agree everywhere with the solid curve in Fig. 8 calculated from Eq. (12) with $\mathcal{E}_c = 2 \pm 0.5$ kV/cm and $\mu_+ = 430 \pm 100$ cm^2/V sec.

The positron drift velocity in diamond, as depicted in the lower graph of Fig. 8, shows no field dependence within the accuracy of the data. The positrons should reach a saturation drift velocity $v_s \simeq (\hbar\omega_0/m_+)^{1/2}$ only at high fields such that $\frac{1}{2}m_+v_d^2$ becomes comparable to the excitation energy $\hbar\omega_0$, of the optical modes of the lattice vibrations, which for Si ($\hbar\omega_0 \simeq 0.1$ eV) and diamond ($\hbar\omega_0 \simeq 0.2$ eV) attains values ~2×10^7 cm/sec. The measured v_d are smaller by two orders of magnitude. The constancy of v_d in our diamond crystal over the limited $\mathcal{E}$ range studied may signify field-enhanced positron defect trapping.

The mobilities, $\mu_+ = e\tau_{sc}/m^*$, of positrons in Si and diamond are 5 to 10 times smaller than the corresponding electron mobilities, although the phonon and defect scattering times τ_{sc} should be essentially the same for both particles. It follows

that, while the effective electron mass is $m_-^* = \frac{1}{5} m_0$ in such crystals, the effective positron mass is $m_+^* \simeq m_0$. This result has important implications for the positron-lattice interaction as compared to the electron-lattice interaction in the respective conduction bands which invite theoretical analysis.[20]

According to the Einstein relation $D_+ = \mu_+(k_B T/e)$, the diffusion constants are $D_+(\mathrm{Si}) \simeq 10 \pm 3$ cm^2/sec and $D_+(\mathrm{diamond}) = 5 \pm 3$ cm^2/sec. Positron lifetime data of Si powders with different grain sizes[21] with $\tau_c = 230$ psec and surface lifetime $\tau_s = 520$ psec yield $D_+(\mathrm{Si}) = 8 \pm 4$ cm^2/sec.[1] Lifetime data on diamond powder[17] give the estimate $D_+(\mathrm{diamond}) = 2 \pm 1$ cm^2/sec.

An experiment was performed on Teflon $(-CF_2-)_n$, to test the consistency of this method with independent measurements of the electric field dependence of positronium (Ps) formation in Teflon[22] which gives the estimate $D_+(CF_2) \sim 10^{-2}$ cm^2/sec. Electric fields across Teflon samples up to $\mathcal{E} = 10^5$ V/cm caused no discernible change of N_1, with an accuracy corresponding to an upper bound $\mu_+(CF_2) \lesssim 2$ cm^2/V sec or $D_+(CF_2) \lesssim 5 \times 10^{-2}$ cm^2/sec.

After this paper was submitted for publication, mobility measurements by the Doppler shift method were reported in Ge, with the results $\mu_+ = 350 \pm 17$ cm^2/V sec at 36 °K and $\mu_+ = 124 \pm 10$ cm^2/V sec at 93 °K,[23] which extrapolates to $\mu_+ \sim 20$ cm^2/V sec at 300 °K. Recent angular correlation measurements on diamond and quartz crystals gave upper μ_+ bounds of 15–20 cm^2/V sec.[24] New data are required to assess the reasons for such differences in results obtained on related substances by different methods.

We explored the possibility of observing, through a shift ΔN_1, the electromigration of positrons in metals in the same direction as the conduction-electron "wind" in high electric currents along the implantation direction. Estimates of positron-electron scattering at metallic densities[1] show, however, that the electromigration of positrons during their lifetime in metals is too short to produce effects that are detectable by this technique. It could perhaps be observed as a variation of the γ-ray Doppler shift of order $2v_{d-}/c$, where v_{d-} is the electron drift velocity.

The experimental positron transport coefficients are summarized in Table III.

TABLE III. Positron mobilities μ_+ and diffusion constants $D_+ = \mu_+(k_B T/e)$.

Material	μ_+ (cm^2/V sec)	D_+ (cm^2/sec) PIPE	D_+ (cm^2/sec) Lifetime
Si [a]	430 ± 100	11 ± 4	8 ± 4 [c]
C (diamond) [a]	160 ± 80	4 ± 2	2 ± 1 [d]
Teflon (CF_2) [b]	≲2	≲5 × 10^{-2}	~1 × 10^{-2} [e]

[a] Single crystal.
[b] Semicrystalline solid.
[c] From powder data in Ref. 21.
[d] From powder data in Ref. 17.
[e] From field-dependent positronium yields (Ref. 22).

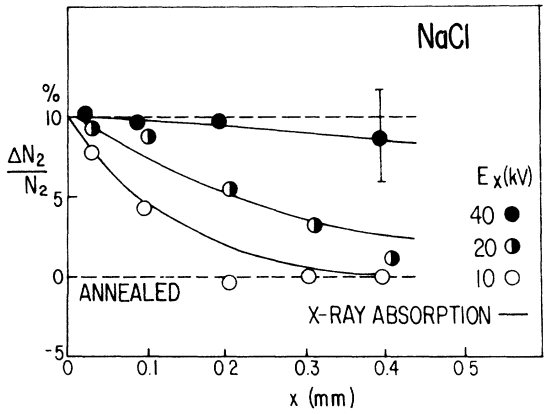

FIG. 9. Mode-2 sweeps of NaCl crystals irradiated with x rays of maximum energy 40, 20, and 10 kV, respectively. The zero reference line represents the M2 profile of the annealed crystals (cf. Fig. 3). For comparison, the curves give the NaCl x-ray absorption for the three x-ray energies. The maximum value, 10%, is typical for saturation changes in the PICA countrate after x irradiation of NaCl (Refs. 25 and 26).

C. Profiles of x-ray induced defects in NaCl

X irradiation produces defects in NaCl that trap positrons to form A centers, where positrons annihilate with a longer mean lifetime and a higher PICA count rate than in the crystal bulk.[25-27] We have measured the depth distribution of x-ray induced A-center precursors for various x-ray energies E_x through changes in the M2 countrate.

Samples cut from a single-crystal NaCl boule were irradiated with x rays for 2 h from a 1-kW W-cathode tube operated at $E_x = 10$, 20, and 40 kV, and the M2 profiles, $N_2^{\mathrm{irr}}(x)$, measured. Each sample was then annealed *in situ* at 450 °C for 2 h, and the M2 profile, $N_2^{\mathrm{ann}}(x)$, recorded in the same geometry with the same positron source. Figure 9 shows the deconvoluted results in the form $\Delta N_2/N_2 \equiv N_2^{\mathrm{irr}}/N_2^{\mathrm{ann}} - 1$ as a function of sample depth x measured from $x_S = 0$. The curves represent the expected x-ray-produced defect concentration profiles as calculated according to $e^{-\alpha_x x}$ with the x-ray mass absorption coefficients, $\alpha_x(E_x)$, of NaCl

for the three values of E_x.

V. SUMMARY

The positrons from ^{64}Cu sources are stopped at mean implantation ranges R_+ corresponding to the same surface density $R_+(0.65\ \text{MeV})d = 34 \pm 2$ mg/cm^2 in solids with d ranging from 0.9 to 9 g/cm^3. The mean implantation range extends deeper, by ~3 mg/cm^2, into a Cu single crystal than in polycrystalline samples. This implies, for example, that ~10% of the positrons penetrate twice as far along the ⟨110⟩ Cu direction than in random directions.

Electric fields $\mathcal{E}$ displace positron implantation-profiles by mean distances $v_d(\mathcal{E})\tau_c$, where v_d is the field-induced positron drift velocity and τ_c the positron lifetime in the crystal bulk. The positron mobilities, $\mu_+ = v_d/\mathcal{E}$, in diamond and Si range from 200 to 400 cm^2/V sec. They are 5–10 times smaller than the corresponding electron mobilities. The effective positron mass in these substances is nearly equal to the electron rest mass.

Defect profiles produced by x rays in NaCl, and their dependence on x-ray energy are measured in terms of the depth-dependent variations of the positron annihilation characteristics that are attributable to A-center formation. Efforts are underway to improve the resolution and sensitivity of the measurements of positron implantation-profile effects.

---

*Work supported by the U. S. NSF and the French Atomic Energy Commission.

†Permanent address: Dept. of Physics, New York University, New York, N. Y. 10003.

[1]W. Brandt, Appl. Phys. 5, 1 (1974).

[2]G. I. Gleason, J. D. Taylor, and D. L. Tabern, Nucleonics 8, 12 (1951).

[3]L. A. Page and M. Heinberg, Phys. Rev. 102, 1545 (1956).

[4]R. Orth, Third International Conference on Positron Annihilation, Otaniemi, Finland, August 1973 (unpublished).

[5]G. Coussot and R. Paulin, J. Appl. Phys. 43, 1325 (1972).

[6]I. K. MacKenzie, C. W. Schulte, T. Jackman, and J. L. Campbell, Phys. Rev. A 7, 135 (1973).

[7]A. T. Stewart, Can. J. Phys. 35, 168 (1957).

[8]This crystal was kindly placed at our disposal by De Beers Diamond Research Laboratories, Johannesburg, South Africa.

[9]This detector was prepared and characterized for this work in the Electronics Laboratory at Saclay, France, under the direction of A. Friant to whom we express our gratitude.

[10]A. T. Nelms, *Energy Loss and Range of Electrons and Positrons*, Nat. Bur. of Stds. Suppl. to Circ. No. 577 (U.S. GPO, Washington, D. C., 1958).

[11]W. Brandt, *Energy Loss and Range of Charged Particles in Compounds* (1960), Document No. 02194 (National Auxiliary Publication Service, 440 Park Ave. S., New York, N. Y. 10016).

[12]G. Lang and S. DeBenedetti, Phys. Rev. 108, 914 (1957).

[13]W. Brandt, in *Proceedings of the International Conference on Positron Annihilation*, 1965, edited by A. T. Stewart and L. O. Roellig (Academic, New York, 1967), p. 175.

[14]E. A. Konorova and S. A. Shevchenko, Sov. Phys.-Semicond. 1, 299 (1967).

[15]P. G. Litovchenko, V. S. Lutsyak, I. G. Kirnas, P. M. Kurilo, and V. M. Nitsovich, Phys. Status Solidi A 21, 419 (1974).

[16]M. Dorikens, C. Dauwe, and L. Dorikens-Vanpraet, Appl. Phys. 4, 271 (1974).

[17]R. Fieschi, A. Gainotti, C. Ghezzi, and M. Manfredi, Phys. Rev. 175, 383 (1968).

[18]W. Shockley, Bell Syst. Tech. J. 30, 990 (1951).

[19]R. A. Smith, *Semiconductors* (Cambridge U.P., London, 1964).

[20]B. Bergersen and T. McMullen, Solid State Commun. 9, 1865 (1971).

[21]A. Gainotti and C. Ghezzi, Phys. Rev. Lett. 24, 349 (1970).

[22]W. Brandt and J. Wilkenfeld, Phys. Rev. B 12, 2579 (1975); 13, 2243 (1976)E.

[23]A. P. Mills and L. Pfeiffer, Phys. Rev. Lett. 36, 1389 (1976).

[24]O. Sueoka and S. Koide, J. Phys. Soc. Jpn. 41, 116 (1976).

[25]W. Brandt, H. F. Waung, and P. W. Levy, Phys. Rev. Lett. 26, 296 (1971).

[26]W. Brandt, G. Coussot, and R. Paulin, Phys. Lett. A 35, 175 (1971).

[27]W. Brandt and R. Paulin, Phys. Rev. B 8, 4125 (1973).